HHS Public Access

Author manuscript

J Biophotonics. Author manuscript; available in PMC 2019 August 01.

Published in final edited form as:

J Biophotonics. 2018 August ; 11(8): e201700126. doi:10.1002/jbio.201700126.

High-speed microscopy for in vivo monitoring of lymph dynamics

Mustafa Sarimollaoglu[1,*], **Amanda J. Stolarz**[2], **Dmitry A. Nedosekin**[1], **Brittney R. Garner**[2], **Terry W. Fletcher**[2], **Ekaterina I. Galanzha**[1], **Nancy J. Rusch**[2], and **Vladimir P. Zharov**[1,*]

[1]Arkansas Nanomedicine Center, University of Arkansas for Medical Sciences, Little Rock, Arkansas

[2]Department of Pharmacology and Toxicology, University of Arkansas for Medical Sciences, Little Rock, Arkansas

Abstract

The lymphatic system contributes to body homeostasis by clearing fluid, lipids, plasma proteins and immune cells from the interstitial space. Many studies have been performed to understand lymphatic function under normal conditions and during disease. Nevertheless, a further improvement in quantification of lymphatic behavior is needed. Here, we present advanced bright-field microscopy for in vivo imaging of lymph vessels (LVs) and automated quantification of lymphatic function at a temporal resolution of 2 milliseconds. Full frame videos were compressed and recorded continuously at up to 540 frames per second. A new edge detection algorithm was used to monitor vessel diameter changes across multiple cross sections, while individual cells in the LVs were tracked to estimate flow velocity. The system performance initially was verified in vitro using 6- and 10-μm microspheres as cell phantoms on slides and in 90-μm diameter tubes at flow velocities up to 4 cm/second. Using an in vivo rat model, we explored the mechanisms of lymphedema after surgical lymphadenectomy of the mesentery. The system revealed reductions of mesenteric LV contraction and flow rate. Thus, the described imaging system may be applicable to the study of lymphatic behavior during therapeutic and surgical interventions, and potentially during lymphatic system diseases.

Graphical Abstract

[*]**Correspondence** Mustafa Sarimollaoglu and Vladimir Zharov, Arkansas Nanomedicine Center, University of Arkansas for Medical Sciences, Little Rock, AR 72205., msarimollaoglu@uams.edu, ZharovVladimirP@uams.edu.

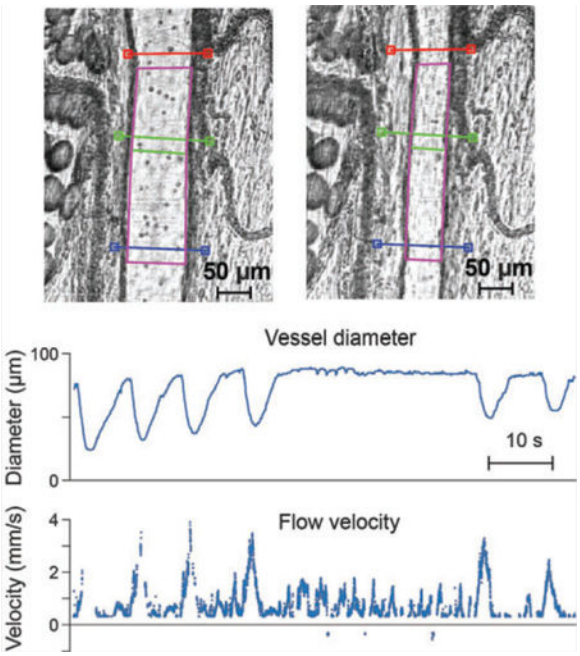

Keywords

video microscopy; cell tracking; contraction; diameter tracking; edge detection; imaging; lymph; lymph flow; lymphedema

1 INTRODUCTION

The mesenteric lymphatic system clears fluid, lipids, plasma proteins and immune cells from the intestinal interstitial space and shuttles them to the venous circulation, thereby contributing to intestinal homeostasis. Conversely, insufficient lymphatic clearance can result in accumulation of immune cells and increase the risk of immune cell-mediated tissue injury leading to chronic inflammation and lymphedema development [1].

The achievements to study these phenomena using optical- and laser-based methods for cytometry of the mesenteric lymph flow in animals can be found elsewhere [2–9]. Several techniques have been used to quantify flow in lymph and blood vessels, including speckle, Doppler [4, 5, 10–12], fluorescence [6, 7] and video microscopy [13–18]. The advanced capabilities of the novel and emerging techniques (eg, speckle, Raman, photothermal and photoacoustic lymph flow cytometry pioneered by our team) were demonstrated by various studies that encompassed vascular and flow dynamics under impacts of pharmaceutics and laser irradiation, lymphatic disturbances from experimental lymphedema and staphylococcal infection, and monitoring of circulating tumor cell trafficking in the lymph system [2–5, 19].

Despite recent significant progress in the field, lymph flow cytometry integrated with assessment of other lymphatic functions (eg, contractility) is still a challenge due to technical limitations. The Doppler method requires many particles in flow, which is not entirely suitable to quantify lymph flow, which contains scarce lymphocytes. Fluorescence

methods rely on injected fluorescent particles that may affect the physiology of the vessel under study. Video microscopy has been used for many years to measure flow and diameter, usually at standard video frame rates of 30 frames per second (fps). However, this low frame rate does not adequately resolve fast moving cells, thereby limiting the flow velocities that can be measured to below ~1 mm/second. Advances in technology (high-speed cameras and increased computing power) offer the opportunity for high frame rate video recording and complex analysis of flow.

Dixon and coworkers measured diameters of lymph vessels (LVs) and the velocity of luminal lymphocytes in situ [8, 9, 20]. These authors achieved frame rates up to 500 fps for several contraction sequences [8], and 300 fps with a resolution of 640 × 480 pixels [20]. Vessel diameter and cells in flow were tracked using image correlation algorithms [21]. More recently, Margaris et al. employed microparticle image velocimetry (PIV) using a pulsed light source [22]. The PIV method relies on tracer particles seeded into flow, thus achieving a higher spatial and temporal resolution of flow measurements. However, this approach is limited to in vitro measurements. Blatter et al. used Doppler optical coherence tomography (OCT) for label-free measurement of lymph flow in vivo [12]. They showed that a Doppler shift can still be detected from very weak signals originating from almost transparent LVs. However, in its current stage, it lacks resolution (250 milliseconds temporal, 11 μm spatial).

The goal of this study was to develop an improved imaging system for continuous monitoring of contractile function of mesenteric LVs and quantification of lymph flow in vivo, which would permit us to evaluate the functional response of the LVs to localized lymphatic insufficiency. Ultimately, the same technology can be used to assess the efficacy of therapeutic strategies to restore lymph flow. Here, we report the design, validation and application of a faster acquisition system and a new processing algorithm to track changes in LV diameter in the rat mesentery and analyze lymph flow in vivo. The acquisition system is capable of compressing and recording high frame rate videos over 500 fps continuously, and for practically unlimited duration. In post processing, instead of using image cross correlation, we detected the changes in diameter of a LV at multiple cross-section lines as a robust way to over-come the limitation of conventional in vivo images. We also tracked lymphocytes individually in the moving lymph fluid, which accounts for flow velocity variations in the ves-sel lumen and enables calculation of volume flow rate.

2 MATERIALS AND METHODS

2.1 Experimental setup

Our experimental setup was built using an Olympus BX51 upright microscope (Olympus America Inc., Center Valley, Pennsylvania; Figure 1). The sample was illuminated by a halogen lamp, and observed through an 8× magnification objective. Field of view was 545 × 545 μm at 8× magnification.

For in vitro verification of the detection system, 90-μm inner diameter glass capillary tubes were used to mimic LVs. Two different sizes of polystyrene microspheres (Polysciences, Inc., Warrington, Pennsylvania), 6.19 ± 0.17 μm and 10.18 ± 0.30 μm (mean ± SD), were

used to mimic red blood cells and white blood cells including lymphocytes, respectively. The flow of particles was provided by a syringe pump (model 780 210; KD Scientific Inc., Holliston, Massachusetts). Flow rate set on the pump was converted to flow velocity in the capillary using the known dimensions. Additionally, particles were fixed on a glass slide and moved by a motorized stage at preprogrammed velocities.

For in vivo measurements, a mesenteric loop was placed on a customized recirculating perfusion chamber (Figure 1) equipped with 2 peristaltic pumps at both inflow and outflow sites to continuously superfuse the mesenteric loop with physiological solution. The stage and objective of the experimental setup were heated (37 °C) to maintain animal body temperature and to prevent condensation, respectively.

2.2 Image acquisition

Video frames were captured by a high-speed camera (model: MV-D1024–160-CL-8; Photonfocus AG, Lachen, Switzerland), and frame grabber (model: microEnable IV AD4-CL; Silicon Software GmbH, Mannheim, Germany). Captured videos were recorded using StreamPix 6 software (NorPix, Inc., Montreal, Canada). Acquisition and postprocessing tasks were performed on a workstation (Precision Tower 7910XL, Dell Inc., Round Rock, TX) with 32GB RAM and an 8 core processor (Xeon E5–2640 v3, Intel, Santa Clara, CA). Video files were compressed in real time using CUDA H.264/AVC encoder module based on a Quadro K2200 (NVIDIA, Santa Clara, California) graphics processing unit, and streamed to an array of hard disk drives in RAID 0 configuration for increased performance.

Compression reduced the video size significantly (~20×), while preserving the image quality (structural similarity index value was 0.9567). Real-time compression combined with continuous streaming to disk array provided virtually unlimited recording capability.

The capability of the acquisition system was tested for several parameters. For the frame size of 512 × 512 pixels, maximum frame capture rate to stream to disk with compression was 540 fps. For a smaller resolution of 128 × 128 pixels, it increased to 1200 fps with compression, and 4000 fps without compression. For the extreme case of 128 × 2 pixels, the maximum rate was 66 000 fps to capture to RAM, and 10 000 fps to stream to hard disk with no compression. Although compression reduced the maximum capture rate of streaming, it still was able to detect cells moving at the expected velocities in LVs under study.

2.3 Image processing

The video analysis program was developed in MATLAB (MathWorks, Natick, Massachusetts) to automatically track LV diameter and lymph flow velocity. A graphical user interface allows the user to browse and play recorded videos at any frame rate, run cell tracking and/or vessel tracking functions, and control all related parameters. The program was designed for minimal user interaction. Setting the initial parameters and selecting a region of interest (ROI) takes only several seconds, and the remainder of the process is done automatically.

2.3.1 Vessel tracking—In a typical in vivo setting, images of rat mesenteric LVs suffer from low contrast and heterogeneity. For instance, adipocytes may block the view of vessel walls, LVs may move out of the focal plane and become obscure during constriction, or blood capillaries may cross over the LVs. To overcome these difficulties and to enable robust and accurate tracking of vessel diameter, we devised the following vessel wall detection algorithm:

A) Place N parallel lines on the image axes. (*N*, the number of cross sections to measure vessel diameter, is defined by the user).

B) User needs to drag and resize the lines to properly cover the ROI on the LV. After any move:

1. Calculate the angle between the line in focus (L_i) and x axis.
2. Retrieve intensity values of pixels along L_i and k-1 more lines that are parallel to L_i, each separated by 1 pixel.
3. Average k line profiles, resulting in L_{iA}.
4. Apply median filter to L_{iA} (filter order should be greater than the cell size to eliminate possible artifacts introduced by passing cells).
5. Detect vessel walls:

a) Split L_{iA} into 3 preliminary regions so that the center region (R_C) covers the vessel, and the left and right regions (R_L, R_R) are on the adjacent tissue (regions are predefined by the user, eg, 20%, 60% and 20% of total length of the line profile).

b) Find median values in these regions; m_L, m_C and m_R.

c) Set 2 threshold values for edge detection as the average of 2 neighboring regions: $T_L = (m_C + m_L)/2$, $T_R = (m_C + m_R)/2$.

d) Set the first point in the direction from center to left edge that is below T_L as the left vessel wall.

e) Set the first point in the direction from center to right edge that is below T_R as the right vessel wall.

1. Connect newly found vessel walls with the other 2 (N−1) vessel walls to form a polygon defining the vessel ROI in the area covered by N lines.
2. Determine vessel orientation and set flow direction marker to indicate vessel angle. It will be updated to flow direction in cell tracking.
3. Display new ROI, L_i and L_{iA} profiles, and update vessel diameter traces (Figure 2).

C) Repeat all steps in (B) when video frame changes or user manipulates a line.

D) Filter diameter traces using a median filter to remove spikes.

During adjustment of the cross-section lines, the metrics and visuals are updated live, so the user can see which settings and positions work accurately, that is, ROI polygon follows the vessel walls (Figure 2).

Using multiple cross-section lines allows us to more accurately record changes in vessel diameter representative of the entire vessel, rather than relying on a single cross-section measurement in a vessel wall that may contract heterogeneously along its length. Another advantage of the multiple cross-section lines across the vessel lumen is to avoid discrete obstructions that may preclude measurement at a single cross section. Finally, phase difference between diameter traces at different points may provide more insight into patterns of contraction along the vessel (Figure 2F).

Flowing objects may be confused with the vessel wall when they have similar contrast. This was especially true for in vitro measurements. Averaging of cross sections helps to reduce these wall detection errors. For instance, some particles under the cross-section lines in Figure 2A appear similar to the tube walls in profile plots (gray dips between vessel walls in Figure 2B). These artifacts are usually eliminated by averaging (colored lines in Figure 2B) or careful selection of threshold parameters. Nevertheless, any remaining artifacts appear as spikes in diameter traces (arrow in Figure 2F). However, since cells move faster than the contracting vessel, these spikes can be filtered out.

The frequency of LV contractions is much slower than the video frame rate, which is targeted to detect fast moving cells within the vessel; 30 fps is usually adequate to track vessel diameter with enough time resolution. Thus, only a subset (5%−10%) of the available video frames is used for vessel tracking to reduce processing time.

2.3.2 Cell tracking—Cell tracking identifies moving cells in the LV and extracts their trajectories from frame to frame. Knowing the inter-frame time and vessel diameter estimated in Section 2.3.1, we can estimate the flow rate. However, the bidirectional and dynamic nature of lymph flow can confound cell tracking. Challenges include that: (1) cells have low contrast in their environment; (2) they may move in and out of focus, thus changing brightness and shape; (3) cells can change velocity (slow down, speed up or stop) and also move in another direction; (4) cell velocities may vary greatly even in the same vicinity; (5) cells usually are only several pixels in diameter, because a large field of view is required for vessel wall tracking and to capture fast moving cells; thus, low magnification is used; (6) cell shape is not suitable for distinguishing one cell from another and cannot be used for predicting the direction of motion.

Fourteen particle tracking methods were quantitatively compared by Chenouard et al. recently [23]. We selected the method by Sbalzarini and Koumoutsakos [24], which performed well for various tasks in this published comparison. Its particle detection implementation is based on an algorithm by Crocker and Grier [25]. We modified it for cell detection and tracking in LVs and devised the following algorithm. In the following, i^{th} frame of a video is represented as a matrix $A_i(x,y)$, where x and y are pixel row and column indices, respectively. There are 3 user-defined parameters: w is the approximate radius of the particles in the images in units of pixels, c is the score cut-off value for nonparticle

discrimination and r is the percentile value that determines which bright pixels are accepted as particles. Subsequently:

A) Define ROI. It is usually the polygon defined by the ves-sel tracking algorithm, which adapts to vessel contraction. Alternatively, user can draw a freeform polygon to define a static ROI.

B) Preprocess the video:

1. Subtract consecutive frames to improve contrast $\left(A_i = A_{i+1} - A_i\right)$. This makes the moving cells visible, while reducing the static background.
2. Mask the frames by setting the pixels outside the relevant ROI to zero.
3. Despeckle the frames using a 2D median filter.
4. Find global maximum (I_{max}) and minimum (I_{min}) intensity values in the video.

C) Detect cells. For each frame:

1. Normalize intensity: $A_i(x,y) = \left(A_i(x,y) - I_{min}\right)/\left(I_{max} - I_{min}\right)$.
2. Apply a convolution filter using the kernel in Eq. (4) [25] for image background extraction and noise removal.
3. Determine the threshold intensity value based on *r*.
4. Dilate the image using a circular mask of radius *w*.
5. Identify particles above threshold.
6. Compute zero- and second-order intensity moments for each particle based on Eqs (6) and (7) in [25].
7. Eliminate particles below *c*.

D) Find trajectories. Identify the same cell across consecutive frames and link these sequential positions into trajectories based on the logistic transportation algorithm described in Reference [26].

E) Calculate flow metrics. Flow direction, flow velocity and flow rate are estimated using the trajectories identified in a frame, as follows:

1. Flow direction is determined as positive or negative, based on the vessel orientation identified in vessel tracking.
2. Average flow velocity at frame i is calculated by $v_i = \Delta x/\Delta t$, where Δx is the average distance traveled between frames i and $i + 1$ by all cells identified by their trajectories crossing these frames, and Δt is interframe time (1/fps).
3. Flow rate at frame i is calculated by $Q_i = 1.25 v_i A$, where $A = \pi d_i^2/4$ is cross-sectional area of the vessel, and d_i is average vessel diameter. Due to complexities of flow velocity distribution in a tube [27], an

average of the velocities observed in the video may not exactly match the average velocity that is needed to calculate flow rate. We experimentally found that $1.25v_i$ is a good approximation.

2.4 Animal preparation

Adult male Sprague Dawley rats were purchased from Harlan Laboratories, Inc. (Indianapolis, Indiana). Animals in this study were used in accordance with protocols approved by the UAMS Institutional Animal Care and Use Committee.

For in vivo measurements, rats were anesthetized with 2.5 L/minute isoflurane. A mesenteric loop was exposed through a small incision along the abdominal midline and placed on the recirculating perfusion chamber. The exposed mesentery was superfused at a rate of ~6 mL/minute with a HEPES-buffered physiological salt solution (HEPES-PSS) of the following composition (mmol/L): NaCl 119, KCl 4.7, $MgSO_4$ 1.17, $CaCl_2$ 1.6, $NaHCO_3$ 24, EDTA 0.026, NaH_2PO_4 1.17, glucose 5.5 and HEPES 5.8. The solution pH was set at 7.4 using NaOH. The temperatures of the perfusion chamber and recirculating solution were monitored using a YSI Tele-thermometer and maintained at 37 °C ± 0.25 °C using a recirculating hot water bath and a glass heat exchanger.

LVs considered ideal for imaging had sections devoid of fat to allow clear visibility of the vessel wall for online diameter measurement. We also avoided traversing blood vessels to decrease interference of blood flow with cell tracking analysis.

2.5 Mesenteric LV ligation

We modified the standard rat model of severe, generalized mesenteric lymphedema, which involves radical surgical resection of the entire mesenteric lymphatic chain and ducts. Instead, in pilot studies in 2 rats, we ligated a single proximal LV draining 1 mesenteric arcade to more closely recapitulate surgical removal of sentinel lymph nodes. In each rat, base-line lymph flow (Day 0) was recorded for 20 minutes in a LV distal to the planned site of surgical ligation (*ligated region*). Then proximal LVs close to regional mesenteric lymph node were ligated using 8–0 to 9–0 monofilament suture (Figure 3). The LVs distal to "lymphadenectomy" and in the remaining mesentery remained intact. Lymph flow was then recorded for 20 minutes on Day 2 post-ligation in the same distal LVs studied on Day 0. LV contractile function also was characterized on Day 0 and Day 2 as described later.

2.6 Isolated LV perfusion

We used diameter measurements in isolated, cannulated LVs to verify that changes in LV contraction observed in vivo using vessel tracking algorithm correlated to abnormal contractile function of isolated LVs. Second-order rat mesenteric LVs (outer diameter, 100–200 μm) were micro-dissected from the ligated region of rats on Day 2 post-ligation and from a similar region of control rats (Day 0). The LVs were cannulated (flow direction, distal to proximal) and pressurized at 4–5 mmHg of intraluminal pressure (no flow) for 60 minutes in a Living Systems perfusion chamber containing PSS of the following composition (in mmol/L): NaCl 119, KCl 4.7, $MgSO_4$ 1.17, $CaCl_2$ 1.6, $NaHCO_3$ 24, NaH_2PO_4 1.17, EDTA 0.026 and 5.5 glucose. The PSS was bubbled with 7% CO_2 to

maintain pH 7.4; chamber temperature was 37 °C. The LVs were equilibrated until they developed rhythmic contractions. Gravity through a PSS reservoir system was used to control pressure, which was monitored via transducers connected to inflow and outflow cannulas. LV outer diameter was continually recorded (3 Hz) using video microscopy equipped with DMTvas edge detection software (Danish Myo Technology A/S, Aarhus, Denmark).

3 RESULTS AND DISCUSSION

3.1 In vitro verification of flow velocity

First verification of the particle tracking algorithm was performed on microspheres of 2 different diameters (Figure 4). Particles were fixed on glass slides (Figure 4A,D,G). The microscope stage was programmed to move the slide at increasing velocities (0.12–5.76 mm/second range, 0.12 mm/second steps) along the same line in an up and down direction. Since the total traveled distance was constant for each step, increasing velocity resulted in chirp-like traces (Figure 4B,E,H). The whole field of view was used as ROI in particle tracking. Recording of the stage movements (red traces) and velocity traces produced by the particle tracking algorithm were compared (Figure 4B,E,H). Root-mean-square error (RMSE) was used as a measure of accuracy and calculated at every velocity setting (Figure 4C,F,I).

The greater RMSE below velocities of 0.48 mm/second can be explained by the following: The velocity for a particle to move 1 pixel in 2 consecutive frames is 0.53 mm/second at the experiment settings (video frame rate = 500 fps, 1 pixel = 1.06 μm). Below this threshold velocity, particles appear to be static in consecutive frames and the algorithm overestimates their velocity. Nevertheless, this threshold is usually below the velocities relevant to cells in LVs [9], and can be overcome by reducing the frame rate in postprocessing.

Average RMSE for $v \geq 0.48$ mm/second was 0.064, 0.094 and 0.089 for 10 μm, 6 μm and mixture of 6 and 10 μm particles, respectively. As expected, smaller particles were more difficult to detect and track, thus resulting in a 47% increase in RMSE.

Next, we tested the particle tracking algorithm using flow through a “vessel” of defined and static diameter. A syringe pump was used to control flow velocity; 10-μm microspheres were diluted in PSS and pumped through a capillary tube (90-μm inner diameter). The syringe pump was set at a flow rate of 0.03 mL/hour, and increased stepwise every 1 minute to a maximum flow rate of 1.5 mL/hour. These endpoint settings translate to 1.0 and 51.5 mm/second flow velocity after accounting for capillary diameter. At these velocities, a particle would traverse 2.0 and 103.0 μm, respectively, between 2 consecutive frames acquired at 500 fps. Since the tube was fixed and stable, diameter traces were constant without any artifacts (Figure 5A). The software was able to accurately detect particles moving at velocities as high as 41 mm/second (Figure 5B). Above this velocity, particle recognition suffered from limited field of view and relatively long camera exposure as the particles appeared as streaks. This deficiency can be resolved by using a higher frame rate and stronger illumination; however, this upper limit of detect-able velocity already is well above

the relevant cell velocities in lymphatics. Conversion to the flow rate using the software also resulted in values closely matched to pump settings (Figure 5C).

A short section of the video represented in Figure 5 was analyzed manually for comparison to automatic cell tracking (Figure 6). Seven particles were identified and tracked along 36 frames (Figure 6A). The calculated velocities based on the distance between their locations in the 1st and 36th frames were 3.58, 5.00, 2.98, 5.71, 3.22, 5.62 and 3.87 mm/second, respectively, for the particles from left to right (Figure 6B). The average velocity was 4.28 ± 1.06 mm/second (mean ± SD, $n = 7$). Track paths for the same particles detected by the software are shown in Figure 6C. Some of the tracks were shorter than the real trajectories, usually due to nearby passing particles confusing the detection. The software measured average velocity for each frame using all the particles detected in the ROI in the relevant frame. The mean value of average velocities in the set of 36 frames was 3.96 ± 0.07 mm/second (mean ± SD, $n = 35$). Although the calculation of cell velocity using software analysis was not exactly the same as manual measurements, the software average velocity values were close to those obtained manually (8% difference) and possibly more accurate.

Next, we used our strategies validated by in vitro methods to track LV diameter and cells for calculation of flow velocity. We assessed lymphatic function using the rat mesenteric lymphatic system in vivo under physiological conditions and after surgical lymphadenectomy, which is a condition associated with impaired LV function and lymphatic insufficiency.

3.2 Measurement of impaired LV contractions and flow velocity during lymphatic insufficiency in vivo

We sought to demonstrate that our improved strategy for high-speed video microscopy could be used to detect abnormalities of LV contraction and lymph flow in vivo. Accordingly, we evaluated these functional parameters in mesenteric LVs distal to surgical lymphadenectomy. We reported earlier that volumetric lymph flow is compromised in the early stage of this condition [19]. Interestingly, Dongaonkar et al. observed that in LV segments isolated from the bovine mesentery subjected to partial lymphatic occlusion for 3 days adapted to become stronger lymphatic pumps, suggesting that prolonged changes in transmural pressure alter the functionality of LVs [28]. Our study sought to measure changes in both lymph flow and contractions in a model of lymphatic insufficiency. In our pilot studies, rats were anesthetized and 1 loop of mesentery was exposed on a heated microscope stage. High-speed optical imaging in vivo was performed on a chosen LV preoperatively and then performed again on Day 2 after LV ligation, enabling each LV to serve as its own control. Using our cell tracking algorithm for calculation of flow rate (Figure 7), our results revealed that average flow rates were reduced severely in the impaired LVs located in the ligated region of both animals as expected (Figure 8A). Flow rate was reduced an average of 85% on Day 2 in LVs distal to the ligated site ($n = 2$). Average flow rate decreased from 0.55 μL/second on Day 0 to 0.05 μL/second on Day 2.

Concurrent with the impairment of lymph flow, we observed severe contractile dysfunction of the affected LVs. Prior to ligation of proximal LVs to mimic lymphadenectomy (as shown in Figure 3A-B), LVs in the ligated region exhibited robust rhythmic contractions (Figure

8B). However, the same LVs exhibited only faint contractions on Day 2 after ligation (Figure 8C), a finding that corresponded to the loss of lymph flow (Figure 8A). Thus, our improved methods allow us to concurrently detect impaired LV contractions and reduced lymph flow rate during lymphatic insufficiency, similar to previous reports by Zolla et al. [29]. Accordingly, our improved methods for assessing lymphatic function may provide a useful preclinical tool to identify mechanisms of lymphatic diseases and evaluate antilymphedema therapeutics designed to normalize LV contractile behavior and lymph flow.

3.3 Confirmation of impaired contractions in isolated LVs

We also verified that contractile behavior in isolated LVs exposed to our model of lymphatic insufficiency showed impaired contractions that corresponded to the loss of contractions observed in LVs of the ligated region, which were recorded for the first time in vivo. For these studies, mesenteric LVs were isolated from control rats or from the ligated region on Day 2 post-ligation. The vessels were cannulated on glass micropipettes and equilibrated in PSS to allow the development of rhythmic contractions. Contractions were regular and robust in LVs from control rats on Day 0 (Figure 9A), whereas LVs dissected from ligated regions on Day 2 showed severely impaired contractions (Figure 9B). Thus, the impaired LV contractions recorded in vivo from rats with lymphatic insufficiency could be recapitulated using isolated LVs, potentially providing complementary preparations in which to explore mechanisms of LV dysfunction.

4 CONCLUSION

Analysis of the contractile behavior of the lymphatic system and quantitation of lymph flow face the challenge of studying a highly dynamic vascular system characterized by phasic contractions, heterogeneous vessels with fast moving cells, and bidirectional flow. While in a static liquid suspension, nanoparticle tracking analysis can be used to accurately analyze particles [30], but it is limited to particles sized below 1 μm. Thus, a different approach was needed to measure flow dynamics in LVs that contain faster-moving and much larger cells. Yet, the lymphatic system, which is sometimes called the third circulation in deference to the better-characterized arterial and venous circulations, is increasingly recognized as a participant in diverse pathologies that include establishment of a tumor microenvironment, inflammation and/or infection at surgical sites and the induction of drug-related lymphedema. By capitalizing on advances in technology to understand the physiological and pathophysiological behavior of the lymphatic system, we will be able to define its contribution to disease states and devise therapeutic interventions to restore normal function.

Here, we provided details about the development and validation of an improved imaging system for continuous monitoring of lymph flow; this system concurrently records lymphatic contractions in vivo. The performance and validity of new algorithms for cell tracking to estimate lymph flow were verified using in vitro tests, which included microparticle tracking in glass capillary tubes and fixed microspheres subjected to known velocities. We were able to postprocess high frame rate bright-field videos of LVs to record diameter and flow velocity in the same vessel, thereby raising the future possibility of identifying patterns of LV contractile behavior that result in deficits of lymph flow. There are

several novel aspects of our approach. First, in contrast to other methods (cross correlation, Doppler OCT, etc.), we track individual cells, so data including shape, size, and location can be assigned to each cell. This single-cell capability is an improvement over the cross-correlation method, for example, which requires multiple cells to be in the window to acquire consistent measurements due to the algorithm's dependency on a certain number of particles in the correlation window [21]. Second, we introduce a new edge detection algorithm, which tracks vessel diameter across multiple cross sections to provide a more integrated picture of vessel contractile behavior and accommodate differences in vessel dimensions in vivo. The multiple diameter measurements allow a better estimation of vessel area compared to single readings and can provide insight into contraction patterns along the vessel. Third, we were able to achieve very high frame rates (over 1000 fps) for continuous streaming and compression, while imaging a 0.5-mm-long LV section in full diameter. We used 500 fps to capture velocities observed in LVs; however, higher frame rates can be used to average consecutive frames and improve signal-to-noise ratio in low-light conditions in vivo, or to accommodate higher velocities in vitro. In contrast, the Doppler OCT method has temporal resolution of 250 milliseconds for flow velocity measurements, and 480 milliseconds for volumetric flow rate measurements [12], whereas our resolution is 2 milliseconds for both (at 500 fps). Fourth, our technical platform can record videos at high frame rates without any stoppage, for practically unlimited (days-long) duration. This capability is due to continuous streaming and real-time compression, and limited only by the computer storage. Overall, our approach is at least comparable to existing methods for estimating velocity and volumetric flow rate, and more versatile as it provides detailed data on single cells. These data can be obtained in vivo without introducing additional markers (ie, dyes, microparticles and fluorescence labels) or more complex modalities.

Ultimately, we demonstrated the ability of our system to detect impaired contractions of LVs and compromised lymph flow in an experimental rat model of regional lymphatic insufficiency. These findings provide "proof of principle" that our improved analysis may be a useful preclinical tool to identify lymphatic dysfunction in different pathological states and search for therapies to restore lymph flow. Although lymphedema is associated with swelling, pain and infection at the affected site, there are no medications to treat it, and patients primarily rely on compressive bandages, pneumatic pumps and other mechanical interventions to minimize complications. This situation emphasizes the pressing need to improve our capabilities to accurately assess the function of the lymphatic system.

ACKNOWLEDGMENTS

Funding for these studies was provided by a UAMS College of Medicine Pilot Grant (N.J.R.), NCI R21 CA187325 from the National Institutes of Health (N.J.R. and E.G.), PhRMA Predoctoral Fellowship (A.J.S.) and Rho Chi AFPE First Year Graduate Fellowship (A.J.S.). This work was also supported in part by the NIH grants R01CA131164 and R01EB017217, the NSF grants OIA 1457888 and DBI 1556068 and a Translational Research Institute grant from UAMS (V.P.Z.).

Funding information

National Cancer Institute, Grant/Award number: NCI R21 1CA131164; National Institutes of Health, Grant/Award numbers: R01CA131164, R01EB017217; National Science Foundation, Grant/Award numbers: OIA 1457888, DBI 1556068; Translational Research Institute grant from UAMS; Rho Chi AFPE First Year Graduate Fellowship; PhRMA Predoctoral Fellowship; UAMS College of Medicine Pilot Grant

REFERENCES

[1]. Ly CL, Kataru RP, Mehrara BJ, Int. J. Mol. Sci 2017, 18, 171.

[2]. Galanzha EI, Tuchin VV, Zharov VP, World J Gastroenterol 2007, 13, 192.

[3]. Galanzha EI, Shashkov EV, Tuchin VV, Zharov VP, Cytometry A 2008, 73A, 884.

[4]. Galanzha EI, Brill GE, Aizu Y, Ulyanov SS, Tuchin VV, Handbook of Optical Biomedical Diagnostics, SPIE Press PM107, Bellingham, WA 2002, p. 875.

[5]. Fedosov IV, Aizu Y, Tuchin VV, Yokoi N, Nishidate I, Zharov VP, Galanzha EI, in Optical Biomedical Diagnostics, Methods, 2nd ed., Vol. 2 (Ed: Tuchin VV), SPIE Press PM263, Bellingham, WA 2016, p. 299.

[6]. Fischer M, Franzeck UK, Herrig I, Costanzo U, Wen S, Shiesser M, Hoffmann U, Bollinger A, Am. J. Physiol 1996, 270, H358. [PubMed: 8769772]

[7]. Leu AJ, Berk DA, Yuan F, Jain RK, Am. J. Physiol 1994, 267, H1507. [PubMed: 7943396]

[8]. Dixon JB, Zawieja DC, Gashev AA, Coté GL, J. Biomed. Opt 2005, 10, 064016. [PubMed: 16409081]

[9]. Dixon JB, Greiner ST, Gashev AA, Cote GL, Moore JE, Zawieja DC, Microcirculation 2006, 13, 597. [PubMed: 16990218]

[10]. Mishina H, Asakura T, Opt. Commun 1974, 11, 99.

[11]. Choi CM, Bennett RG, Dermatol. Surg 2003, 29, 272. [PubMed: 12614422]

[12]. Blatter C, Meijer EFJ, Nam AS, Jones D, Bouma BE, Padera TP, Vakoc BJ, Sci. Rep 2016, 6, 29035. [PubMed: 27377852]

[13]. Zawieja DC, Davis KL, Schuster R, Hinds WM, Granger HJ, Am. J. Physiol 1993, 264, H1283. [PubMed: 8476104]

[14]. Li X, Su M, West CA, He C, Swanson SJ, Secomb TW, Mentzer SJ, Dev. Biol 2001, 37, 599.

[15]. Fagrell B, Fronek A, Intaglietta M, Am. J. Physiol 1977, 233, H318. [PubMed: 888975]

[16]. Kassis T, Yarlagadda SC, Kohan AB, Tso P, Breedveld V, Dixon JB, Am. J. Physiol. Gastrointest. Liver Physiol 2016, 310, G776. [PubMed: 26968208]

[17]. Rahbar E, Akl T, Coté GL, Moore JE, Jr., Zawieja DC, Microcirculation 2014, 21, 359. [PubMed: 24397756]

[18]. Akl TJ, Nepiyushchikh ZV, Gashev AA, Zawieja DC, Cot GL, J. Biomed. Opt 2011, 16, 026016. [PubMed: 21361700]

[19]. Galanzha EI, Tuchin VV, Zharov VP, Lymphat. Res. Biol 2007, 5, 11. [PubMed: 17508899]

[20]. Kassis T, Kohan AB, Weiler MJ, Nipper ME, Cornelius R, Tso P, Dixon JB, J. Biomed. Opt 2012, 17, 086005. [PubMed: 23224192]

[21]. Dixon JB, Gashev AA, Zawieja DC, Moore JE, Jr., Coté GL, Ann. Biomed. Eng 2007, 35, 387. [PubMed: 17151922]

[22]. Margaris KN, Nepiyushchikh Z, Zawieja DC, Moore J, Jr., Black RA, J. Biomed. Opt 2016, 21, 025002.

[23]. Chenouard N, Smal I, de Chaumont F, Maška M, Sbalzarini IF, Gong Y, Cardinale J, Carthel C, Coraluppi S, Winter M, Cohen AR, Godinez WJ, Rohr K, Kalaidzidis Y, Liang L, Duncan J, Shen H, Xu Y, Magnusson KEG, Jaldén J, Blau HM, Paul-Gilloteaux P, Roudot P, Kervrann C, Waharte F, Tinevez J, Shorte SL, Willemse J, Celler K, van Wezel GP, Dan H, Tsai Y, de Solórzano CO, Olivo-Marin J, Meijering E, Nat. Methods 2014, 11, 281. [PubMed: 24441936]

[24]. Sbalzarini IF, Koumoutsakos P, J. Struct. Biol 2005, 151, 182. [PubMed: 16043363]

[25]. Crocker JC, Grier DG, J. Colloid Interface Sci 1996, 179, 298.

[26]. Dalziel SB, Appl. Sci. Res 1992, 49, 217.

[27]. Ortiz D, Briceño JC, Cabrales P, Physiol. Meas 2014, 35, 351. [PubMed: 24480871]

[28]. Dongaonkar RM, Nguyen TL, Quick CM, Hardy J, Laine GA, Wilson E, Stewart RH, Am. J. Physiol. Heart Circ. Physiol 2013, 305, H203. [PubMed: 23666672]

[29]. Zolla V, Nizamutdinova IT, Scharf B, Clement CC, Maejima D, Akl T, Nagai T, Luciani P, Leroux J-C, Halin C, Stukes S, Tiwari S, Casadevall A, Jacobs WR, Jr, Entenberg D, Zawieja

DC, Condeelis J, Fooksman DR, Gashev AA, Santambrogio L, Aging Cell 2015, 14, 582. [PubMed: 25982749]

[30]. Filipe V, Hawe A, Jiskoot W, Pharm. Res 2010, 27, 796. [PubMed: 20204471]

[31]. Sarimollaoglu M, Stolarz AJ, Nedosekin DA, et al. High-speed microscopy for in vivo monitoring of lymph dynamics. J. Biophotonics 2018;11:e201700126 10.1002/jbio.201700126 [PubMed: 29232054]

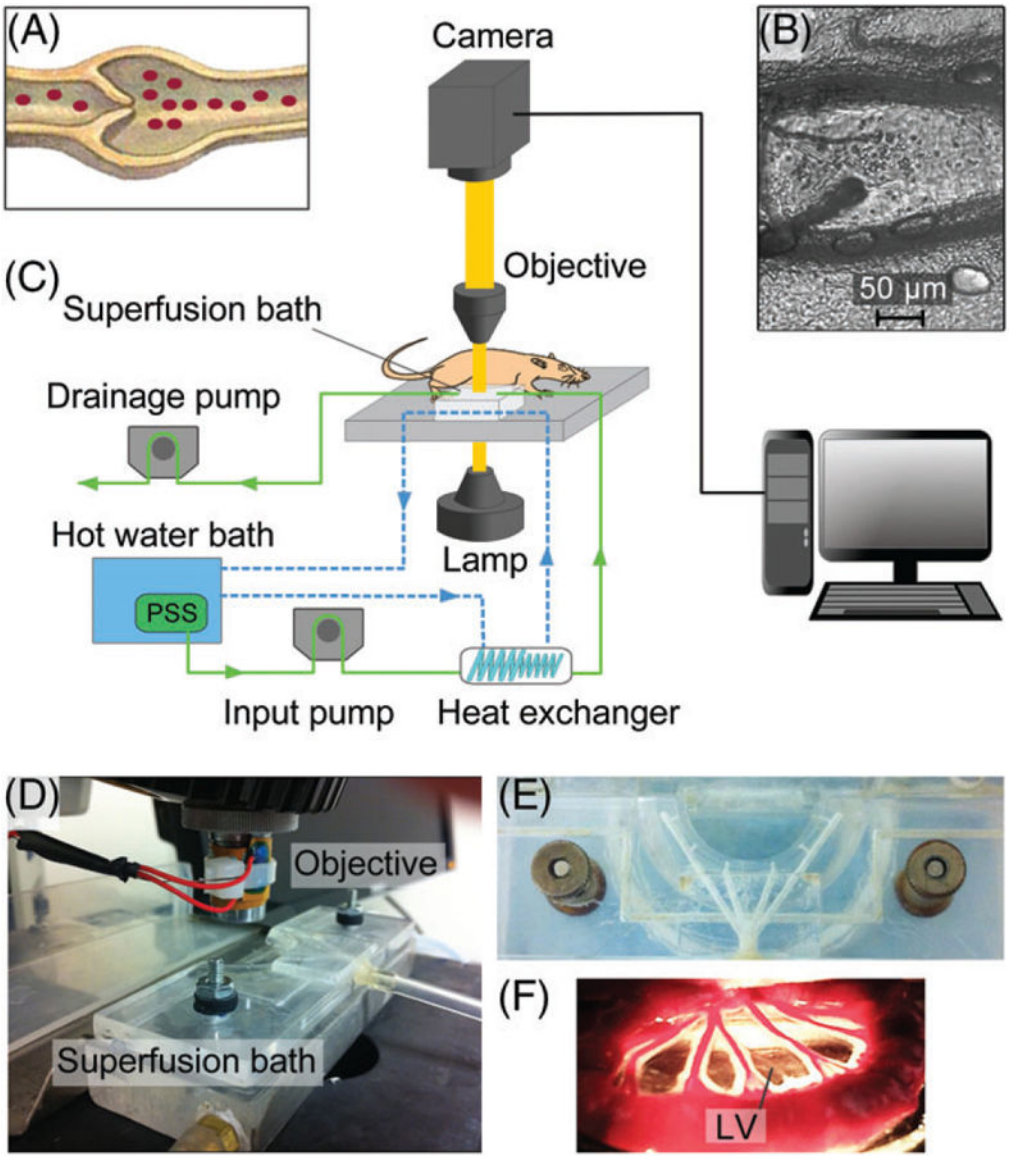

FIGURE 1.

Video microscopy system. (A,B) depiction and real-life image of lymphatic vessels with valves. (C) Light source illuminates the sample. Images captured by the camera are transferred to computer for analysis. A recirculating hot water bath (50 °C) was used to heat the physiological salt solution (PSS) and superfusion bath (37 °C). PSS was actively pumped into, and drained from, the superfusion bath using 2 adjustable peristaltic pumps. A heat exchanger was placed inline of superfusion to prevent temperature loss. (D) the superfusion bath was placed on a microscope stage to visualize LVs. (E) Top view of superfusion bath with perfusion channels. (F) Sample image of LV from exposed rat mesentery

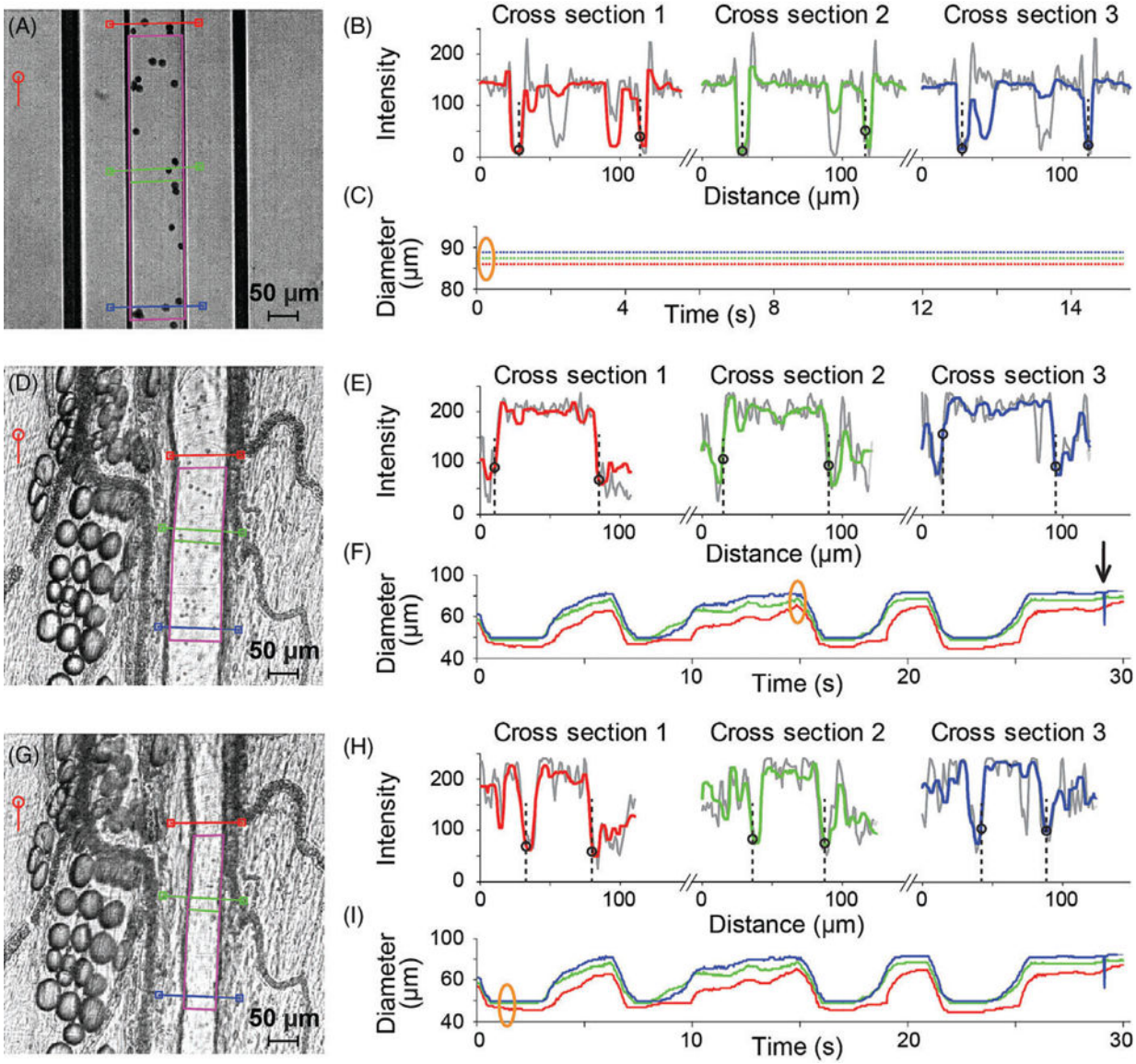

FIGURE 2.

Vessel wall detection and tracking. A glass tube with an inner diameter of 90 μm (A), and a sample tissue in vivo containing a rat mesenteric LV at rest (D) and during contraction (G). $N = 3$ cross-section lines (red, green and blue) were placed and adjusted over a ROI on the image. Automatically detected ROI is indicated by a purple polygon on the image. Red marker indicates the angle and direction of flow, which is automatically derived from the ROI polygon. (B,E,H) Intensities along the cross-section lines and their averaged versions (L_{iA}) plotted in gray (average), red, green and blue, respectively. Black circles and dashed lines indicate the points detected as vessel walls. (C,F,I) Vessel diameter traces show the detected diameters throughout the video. Yellow circles indicate the current frame plotted

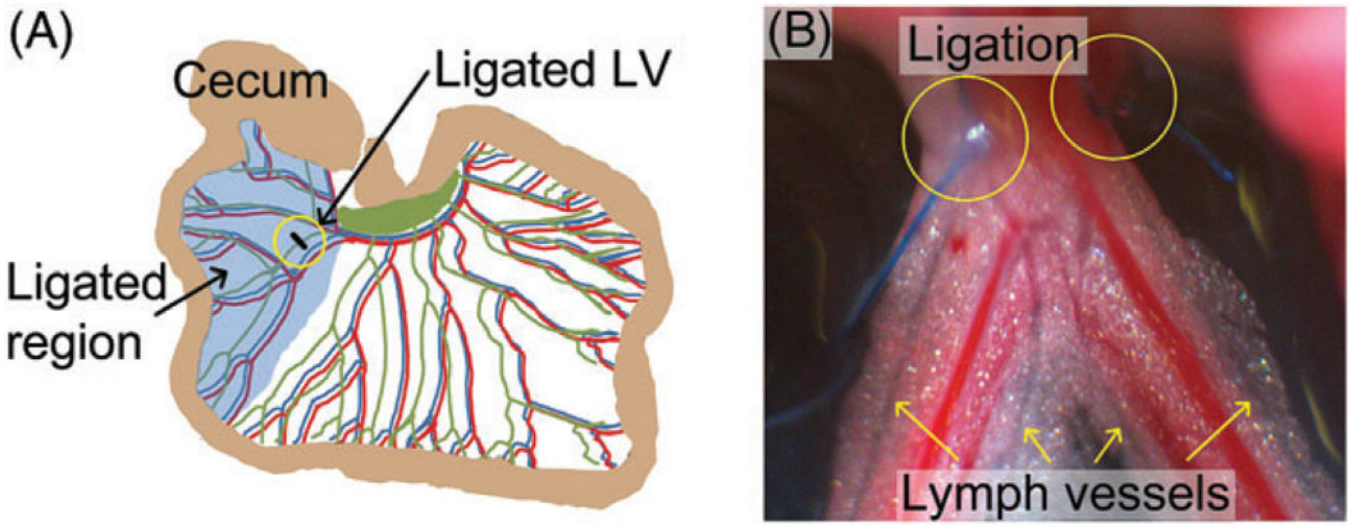

FIGURE 3.

Surgical ligation of proximal rat mesenteric LVs to establish lymphatic insufficiency. (A) Schematic of the site of lymphatic insufficiency after ligation of proximal arcade LVs. (B) Image of ligated LVs (in yellow circles) and distal LVs (yellow arrows) that were subjected to analysis before (Day 0) and 2 days after (Day 2) the ligation

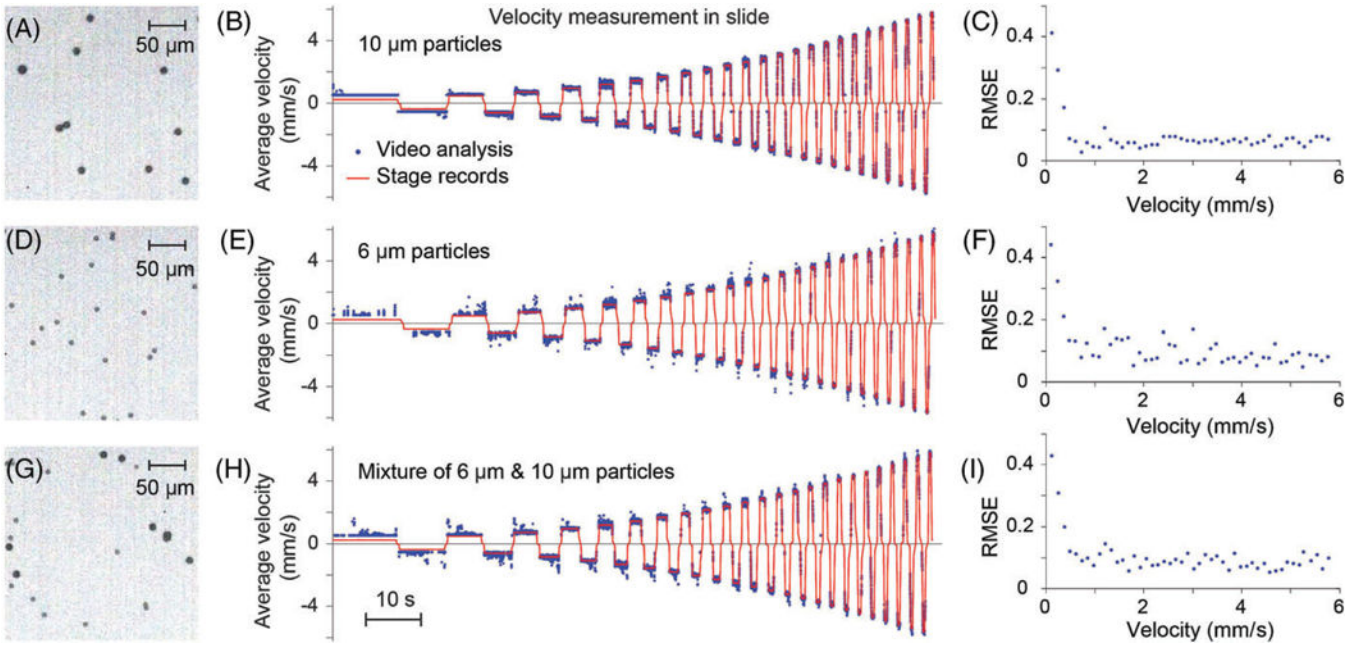

FIGURE 4.

Verification of velocity measurement using the particle tracking algorithm. (A) 10 µm, (D) 6 µm and (G) mixture of 6 and 10 µm microspheres were fixed on slides. One quarter of the total field of view is shown. (B,E,H) Microscope stage was moved in increasing velocities while video was recorded at 500 fps. Set (red) and measured (blue) velocities were traced. (C,F,I) RMSE at each set velocity

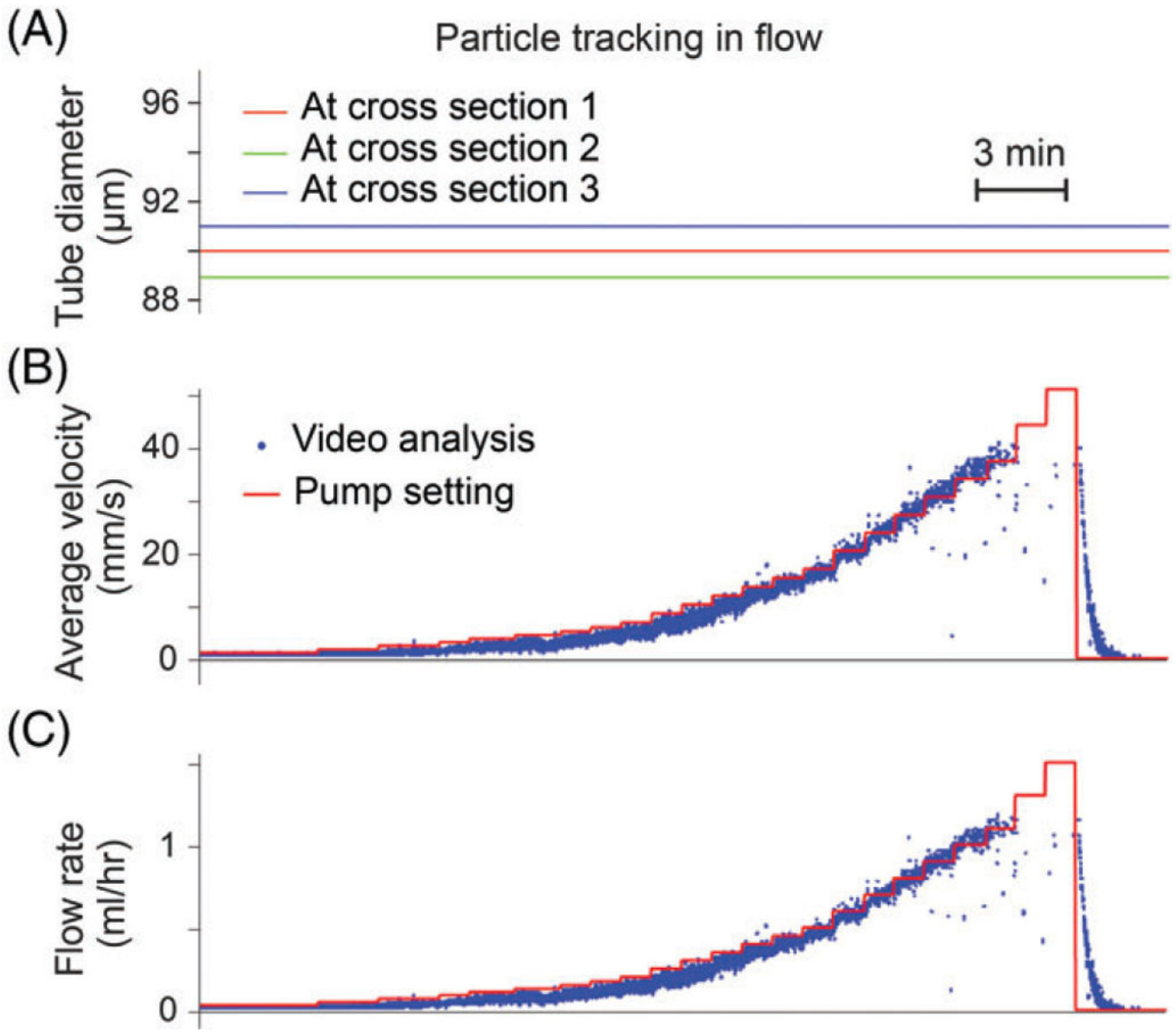

FIGURE 5.

Verification using an in vitro flow model of vessel and cell tracking algorithms. (A) Diameter traces recorded from a glass capillary tube of 90-μm inner diameter. (B) Measured (blue) and set (red) flow velocities of 10-μm diameter microspheres. (C) Flow rate estimated from flow velocity. Video frame rate was 500 fps

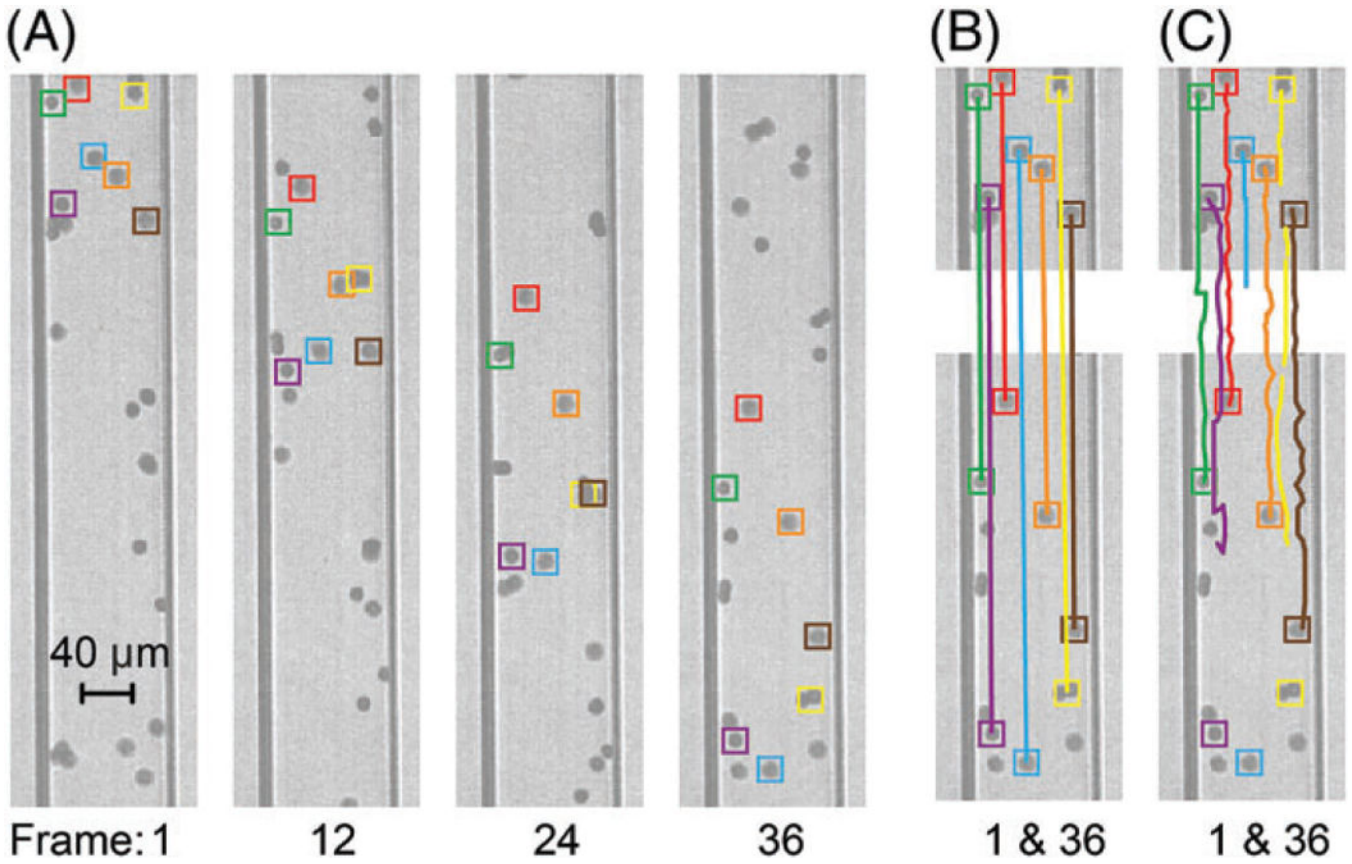

FIGURE 6.

Manual verification of cell tracking algorithm. (A) Seven particles were manually identified and tracked in 36 frames. (B) Their positions in frames 1 and 36 were linked into trajectories shown as colored lines. (C) Trajectories of same particles estimated by the algorithm. Intensity of images is reduced for better visualization of tracking lines. Intermediate frames are not shown. Video frame rate was 500 fps

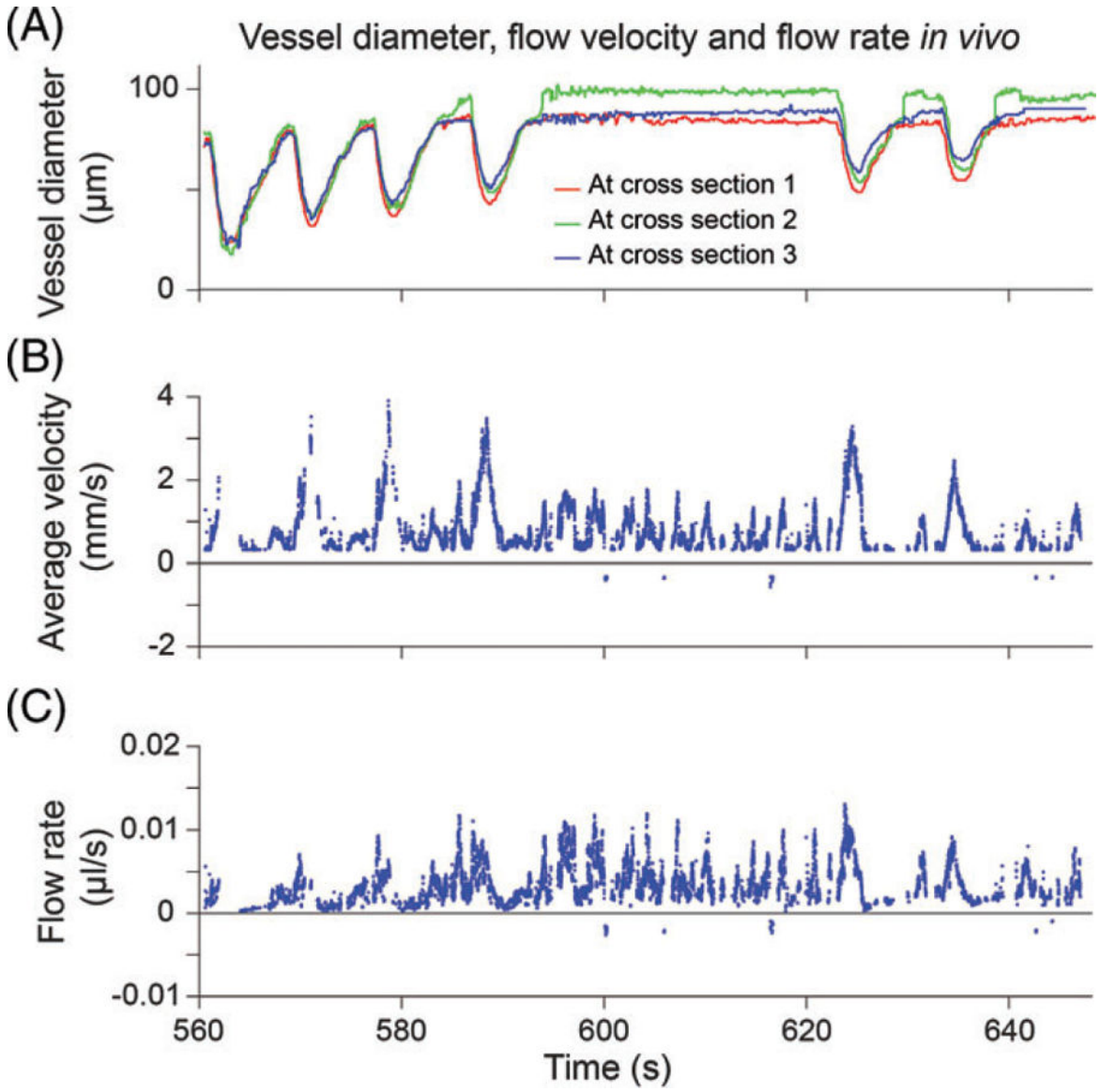

FIGURE 7.

Example snippet from in vivo measurements showing temporal variation of vessel diameter. (A) LV diameter traces at 3 cross-section lines. (B) Average flow velocity in the ROI. (C) Flow rate estimation

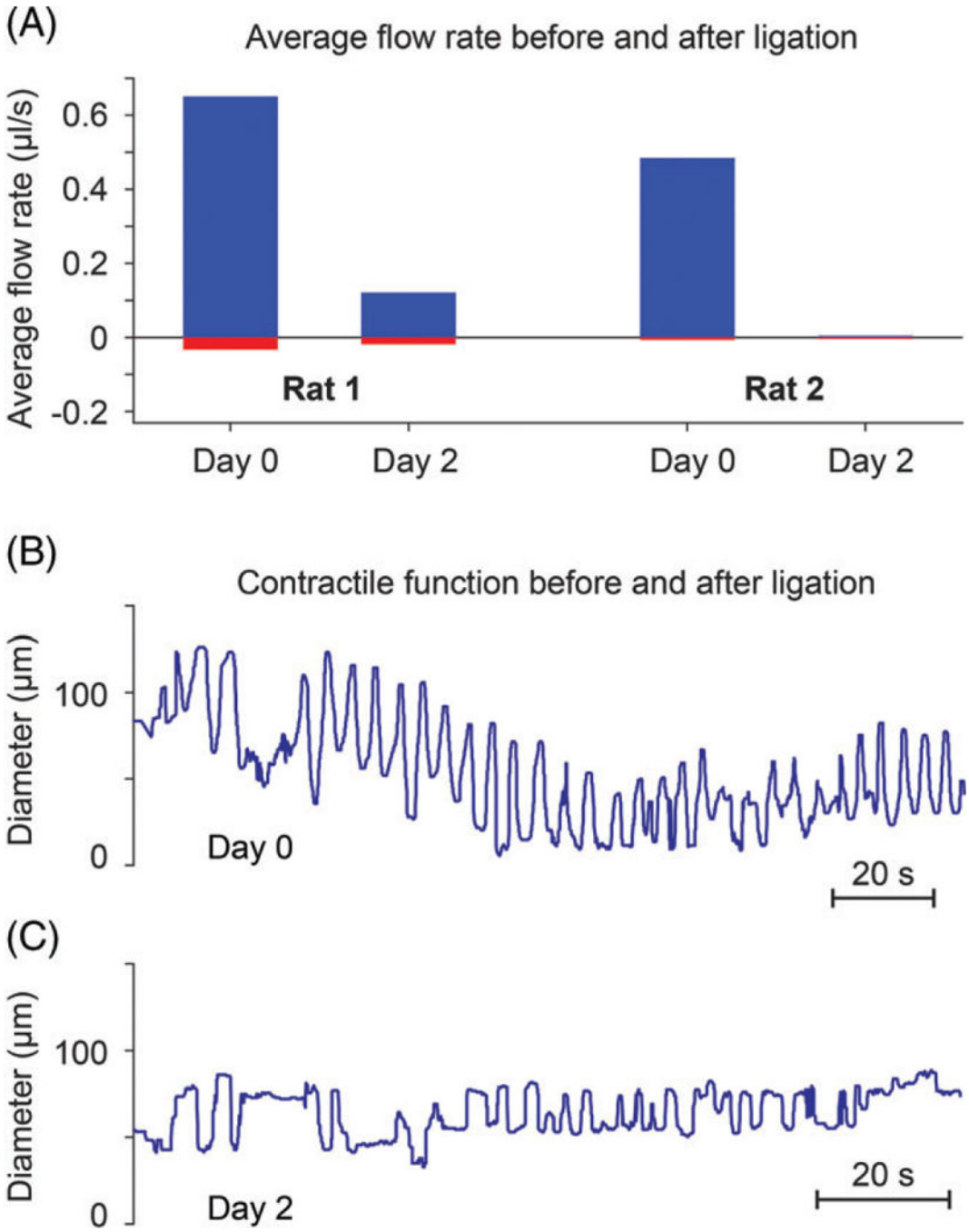

FIGURE 8.

In vivo recordings show loss of lymph flow and contractile dysfunction in LVs from the ligated mesenteric region on Day 2 after surgical ligation of proximal LVs to establish lymphatic insufficiency. (A) Positive flow rate estimated in LVs in the ligated region of 2 different rats on Day 0 (baseline) and Day 2 after ligation. Flow rate was reduced by an average of 85%. (B) Rhythmic contractions recorded from rat mesenteric LVs in vivo without surgery (Day 0). (C) Impaired contractions were observed on Day 2 post-ligation

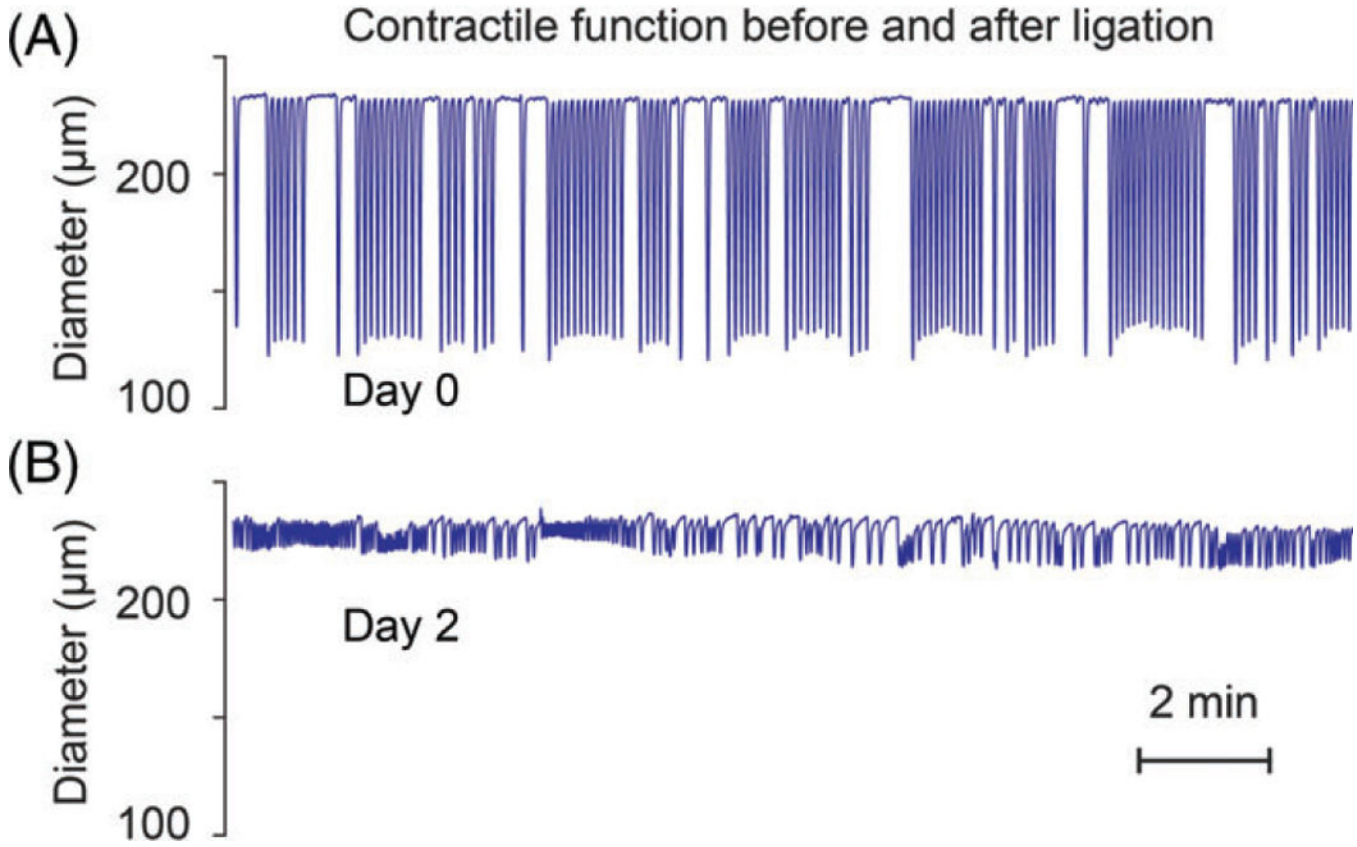

FIGURE 9.

Contractile dysfunction of mesenteric LVs after proximal LV ligation to induce lymphatic insufficiency. (A) Robust rhythmic contractions recorded from mesenteric LVs dissected from rats without surgery (Day 0). (B) Mesenteric LVs dissected on Day 2 from the ligated region exhibit severely reduced contractile amplitude